

The Effect of Harmonic Detection Speed on the Overall Performance of Shunt Active Power Filters

MAHMOUD FAWZY SHOUSHA, SHERIF AHMED ZAID, OSAMA AHMED MAHGOUB

Department of Electrical Power and Machines

Cairo University

Egypt

mahmoudfawzy@ieee.org, sherifzaid3@gmail.com, osamamahgoub@ieee.org

Abstract: - Active Power Filters (APFs) are the up-to-date solution to power quality problems. Shunt active filters (the most common type) allow the compensation of current harmonics, unbalance, together with power factor correction, and can be much better solution than the conventional approach. Harmonic reference detection is the key word for the proper operation of APF. This paper studies the effect of the speed and the complexity of the detection algorithm on the overall performance of the shunt APF. An experimental shunt APF is built and controlled using a Digital Signal Processor (DSP). Three different detection algorithms are analyzed and tested. These algorithms are the Instantaneous Reactive Power Theory (IRPT) or simply the p-q theory, Synchronous Reference Frame (SRF), and Synchronous Detection Method (SDM). The three different extraction techniques result finally in a graded performance of the shunt APF which lead to different results for the supply current THD% and supply power factor.

Key-Words: - Shunt APF, DSP, harmonic detection, IRPT, SDM, SRF.

1 Introduction

Over the recent years, power quality has been given attention due to the intensive use of power electronic controlled applications in all branches of industry, such as controlling or converting A.C. power to feed electrical loads. As a result, harmonics are generated from the power converters or non-linear loads that cause the power system to operate with low power factor, low efficiency, voltage and current distortions, and increased losses in transmission and distribution lines. There are a lot of life examples on such non-linear loads that are widely used ranging from high power industrial applications such as arc furnaces, arc welders, and HVDC to low power domestic applications such as discharge lamps, T.V-sets, computers, fax machines, and printers. Conventionally, passive LC filters [1] are used to eliminate the line current harmonics and improve the P.F. Passive filter have several disadvantages such as the impact of the supply impedance on the passive filter characteristics, resonance problems which may cause the amplification of the line currents at the supply side at specific frequency, the bulk size of the passive filter, and finally the passive filter performance becomes bad in case of load changing.

In order to overcome the disadvantages of the passive filters, APFs are investigated and researched [2]. Nowadays, APFs are widely used in different configurations [3]-[5].

Shunt APF compensates current harmonics by injecting equal-but-opposite harmonic compensating currents. In this case, the shunt APF operates as a current source injecting the opposite harmonic components generated by the load. In this way, the power distribution system sees the non linear load and the APF as an ideal resistor. APF components are shown in Fig.1.

One of the most discussed software part (in the case of DSP implementations) of APF is the harmonic detection method [6]-[11], [23-24]. In brief, it represents the part that is responsible for calculating the information of the measured or estimated signals (voltage, current, power). This information can be (frequency, amplitude, phase shift, harmonic content, etc...). Two different directions are introduced in literature, the time-domain and the frequency-domain methods, frequency domain approaches [13]-[16] can be classified to Fast Fourier Transform (FFT), Discrete Fourier Transform (DFT), and recursive Discrete Fourier Transform (RDFT).

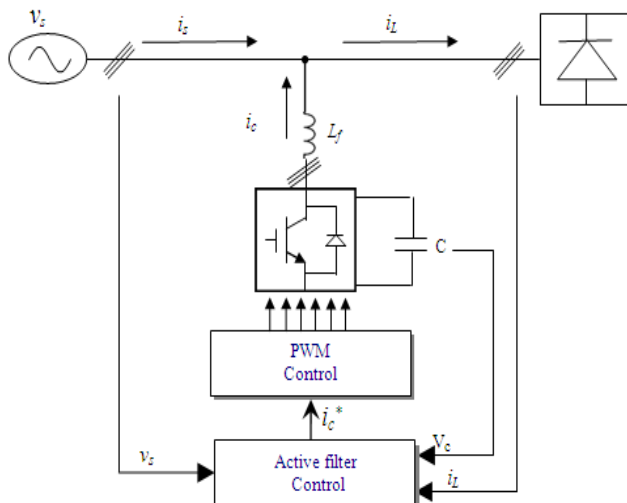


Fig.1. block diagram of APF system

The time-domain methods are mainly used to gain more speed or fewer calculations compared to the frequency-domain methods. Time domain approaches may be classified as Instantaneous Reactive Power Theory (IRPT) or simply the p-q theory, Synchronous Reference Frame (SRF), Synchronous Harmonic Frame (SHF), Synchronous Detection Method (SDM), Fryze power, and generalized integrator. The instantaneous reactive power theory by Akagi et al [17], [18] and the expansion from 3-wire system to 4-wire system by Aredes et al [19] are considered the milestone of the APFs. In this paper, the speed of the detection is measured by measuring the minimum possible sampling time that can be achieved using a specific controller as mentioned in details in section VI.

2 IRPT Theory

The p-q theory is based upon algebraic transformation which transforms the measured voltages and currents from the conventional a-b-c frame to α - β frame as follows:

$$\begin{bmatrix} v_0 \\ v_\alpha \\ v_\beta \end{bmatrix} = \sqrt{\frac{2}{3}} \begin{bmatrix} \frac{1}{\sqrt{2}} & \frac{1}{\sqrt{2}} & \frac{1}{\sqrt{2}} \\ 1 & -\frac{1}{2} & -\frac{1}{2} \\ 0 & -\frac{\sqrt{3}}{2} & \frac{\sqrt{3}}{2} \end{bmatrix} \begin{bmatrix} v_a \\ v_b \\ v_c \end{bmatrix} \quad (1)$$

$$\begin{bmatrix} i_0 \\ i_\alpha \\ i_\beta \end{bmatrix} = \sqrt{\frac{2}{3}} \begin{bmatrix} \frac{1}{\sqrt{2}} & \frac{1}{\sqrt{2}} & \frac{1}{\sqrt{2}} \\ 1 & -\frac{1}{2} & -\frac{1}{2} \\ 0 & -\frac{\sqrt{3}}{2} & \frac{\sqrt{3}}{2} \end{bmatrix} \begin{bmatrix} i_a \\ i_b \\ i_c \end{bmatrix} \quad (2)$$

In case of 3-wire system both v_0 and i_0 equal zero, as i_α and i_β are orthogonal, and the same for v_α and v_β

$$i = i_\alpha + j i_\beta \quad (3)$$

$$v = v_\alpha + j v_\beta \quad (4)$$

$$s = v \times i^* \quad (5)$$

$$\begin{bmatrix} p(t) \\ q(t) \end{bmatrix} = \begin{bmatrix} v_\alpha & v_\beta \\ v_\beta & -v_\alpha \end{bmatrix} \begin{bmatrix} i_\alpha \\ i_\beta \end{bmatrix} \quad (6)$$

Where, $p(t)$ is the instantaneous active power and $q(t)$ is the instantaneous reactive power.

$$p(t) = \bar{p} + \tilde{p} \quad (7)$$

$$q(t) = \bar{q} + \tilde{q} \quad (8)$$

\bar{p} - Mean value of the instantaneous real power:

It corresponds to the transferred energy per time unit from the power source to the load, through a - b - c phases of the three-phase system which equals the conventional active power in three phase system $p = 3VI_1 \cos\phi_1$.

\tilde{p} - Alternated value of the instantaneous real power:

It corresponds to the energy per time unit that is exchanged between the power source and the load, through a - b - c phases.

$q(t)$ - Instantaneous imaginary power:

It corresponds to the power that has to circulate between the phases a - b - c of the three-phase power system (it does not contribute to any energy transfer from power to load, but produces undesirable currents). The average value is the conventional reactive power $= 3VI_1 \sin\phi_1$. Fig.2 shows the power components.

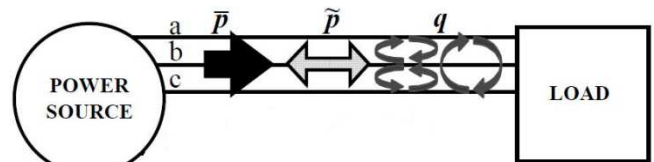


Fig.2. the power components of the p-q theory

In case of 3-wire system, from all the power components of the p-q theory (in case of power factor correction), only the mean value of the instantaneous real power (\bar{p}) is the main concern, because it effectively transfers energy to the load.

One important point to be noticed is the selective behavior [20] of the p-q theory. Harmonic currents

can be only compensated without reactive power compensation, vice versa, or complete compensation. That in turn gives a space to the inverter as it reduces the loading on it, or in other words the inverter rating can be reduced from the beginning.

Performing the inverse of the matrix in (5)

$$\begin{bmatrix} i_{\alpha}^* \\ i_{\beta}^* \end{bmatrix} = \frac{1}{\Delta} \begin{bmatrix} v_{\beta} & v_{\alpha} \\ v_{\alpha} & -v_{\beta} \end{bmatrix} \begin{bmatrix} p \\ q \end{bmatrix} \quad (9)$$

Where; Δ is the voltage norm = $v_{\alpha}^2 + v_{\beta}^2$

In order to calculate the reference currents in $\alpha - \beta$ frame, p and q are replaced by the desired components.

$$\begin{bmatrix} i_{\alpha}^* \\ i_{\beta}^* \end{bmatrix} = \frac{1}{\Delta} \begin{bmatrix} v_{\beta} & v_{\alpha} \\ v_{\alpha} & -v_{\beta} \end{bmatrix} \begin{bmatrix} p^* \\ q^* \end{bmatrix} \quad (10)$$

To obtain the reference currents in the a-b-c frame the inverse Clarke transformation is applied as follows

$$\begin{bmatrix} i_a^* \\ i_b^* \\ i_c^* \end{bmatrix} = \sqrt{\frac{2}{3}} \begin{bmatrix} 1 & 0 \\ -\frac{1}{2} & \frac{\sqrt{3}}{2} \\ -\frac{1}{2} & -\frac{\sqrt{3}}{2} \end{bmatrix} \begin{bmatrix} i_{\alpha}^* \\ i_{\beta}^* \end{bmatrix} \quad (11)$$

Where; i_a^* , i_b^* , and i_c^* is the reference compensator currents in the a-b-c frame and i_{α}^* , i_{β}^* are the reference currents in the α - β frame. For the purpose of complete compensation (i.e. unity P.F.), and exploiting indirect current control, $p^* = \bar{p}$, $q^* = 0$. Figure 3 shows the block diagram of the IRPT.

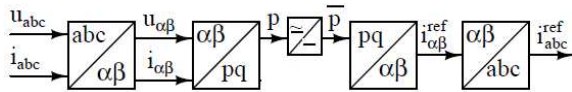


Fig.3 block diagram of the IRPT

3 Synchronous Reference Frame (SRF)

SRF [21] is based on using Clarke transformation at first to transform a-b-c currents to α - β currents

$$\begin{bmatrix} i_{\alpha} \\ i_{\beta} \end{bmatrix} = \sqrt{\frac{2}{3}} \begin{bmatrix} 1 & -\frac{1}{2} & -\frac{1}{2} \\ 0 & -\frac{\sqrt{3}}{2} & \frac{\sqrt{3}}{2} \end{bmatrix} \begin{bmatrix} i_a \\ i_b \\ i_c \end{bmatrix} \quad (12)$$

Then, transformed to d-q axis using Park transformation;

$$\begin{bmatrix} i_d \\ i_q \end{bmatrix} = \begin{bmatrix} \cos\omega t & \sin\omega t \\ -\sin\omega t & \cos\omega t \end{bmatrix} \begin{bmatrix} i_{\alpha} \\ i_{\beta} \end{bmatrix} \quad (13)$$

Inverse Clarke and inverse Park transformations are applied in 14 and 15;

$$\begin{bmatrix} i^*_{\alpha} \\ i^*_{\beta} \end{bmatrix} = \begin{bmatrix} \cos\omega t & -\sin\omega t \\ \sin\omega t & \cos\omega t \end{bmatrix} \begin{bmatrix} i^*_{d} \\ i^*_{q} \end{bmatrix} \quad (14)$$

$$\begin{bmatrix} i^*_{\alpha} \\ i^*_{\beta} \end{bmatrix} = \sqrt{\frac{2}{3}} \begin{bmatrix} 1 & 0 \\ -\frac{1}{2} & \frac{\sqrt{3}}{2} \\ -\frac{1}{2} & -\frac{\sqrt{3}}{2} \end{bmatrix} \begin{bmatrix} i^*_{d} \\ i^*_{q} \end{bmatrix} \quad (15)$$

As for the IRPT, the current in d-q frame can be composed by the instantaneous current $i_q = \bar{i}_q + \tilde{i}_q$ and the instantaneous current $i_d = \bar{i}_d + \tilde{i}_d$. The division of the dc and ac can be obtained using a low-pass filter. Figure 4 shows its block diagram.

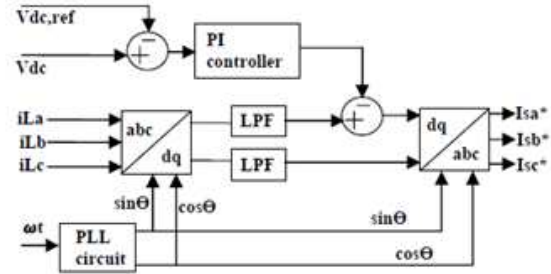


Fig.4 block diagram of the SFR algorithm

4 Synchronous Detection Method (SDM)

SDM method [22] is basically used for the determination of amplitude of the source currents. The instantaneous real power $p(t)$ consumed by the load could be calculated from the instantaneous voltages and load currents as;

$$p(t) = v_{sa}(t) * i_{la}(t) + v_{sb}(t) * i_{lb}(t) + v_{sc}(t) * i_{lc}(t) \quad (16)$$

Where, $v_{sa}(t)$, $v_{sb}(t)$, and $v_{sc}(t)$ are the instantaneous values of supply voltages, and $i_{la}(t)$, $i_{lb}(t)$, and $i_{lc}(t)$ are the instantaneous values of load currents.

The average value P_{dc} is determined by applying $p(t)$ to a low pass filter. The real power is then split into the three phases as follows:

$$p_a = \frac{P_{dc} * V_{sma}}{V_{sma} + V_{smb} + V_{smc}} \quad (17)$$

$$p_b = \frac{P_{dc} * V_{smb}}{V_{sma} + V_{smb} + V_{smc}} \quad (18)$$

$$p_c = \frac{P_{dc} * V_{smc}}{V_{sma} + V_{smb} + V_{smc}} \quad (19)$$

Thus, for three phase ideal supply voltages;

$$p_a = p_b = p_c = \frac{P_{dc}}{3} \quad (20)$$

From (17), (18), and (19) the reference supply currents can be easily determined as follows:

$$i_{sa}^* = \frac{2 v_{sa}(t) * p_a}{V_{sma}^2} \quad (21)$$

$$i_{sb}^* = \frac{2 v_{sb}(t) * p_b}{V_{smb}^2} \quad (22)$$

$$i_{sc}^* = \frac{2 v_{sc}(t) * p_c}{V_{smc}^2} \quad (23)$$

5 Experimental Setup

The hardware setup can be classified into two categories. First, the power circuits which are the following:-

1) Three phase Voltage Source Inverter (VSI) which consists of three IGBT (TOSHIBA MIG200Q2CSB1X) intelligent modules (includes short circuit protection) as shown in Fig.5. The three phase VSI is used to inject the harmonic currents into the Point of Common Coupling (PCC). The load is taken as a three phase uncontrolled bridge rectifier with a resistive load of 24Ω in the D.C. side.

2) Filter inductors at the A.C. side of the three phase VSI. The filter inductors are taken as $5mH$ which is a combination of two inductors of $10mH$ each as shown in Fig.6.

3) D.C. bus capacitors at the D.C. side of the three phase inverter. The capacitors are taken as $930\mu F$ from parallel combination as shown in Fig.7. The second part is the control circuits which comprise the following:

- Current measuring circuit.
- Voltage measuring circuit.
- Conditioning circuit.
- Opto-couplers and isolated power supplies.
- Digital Signal Processor (DSP).

Regarding the current measuring circuit, almost all control algorithms used in Shunt APFs require four current measurements. The first two current sensors are used to measure the load currents in two phases and the third phase current can be easily obtained in case of balanced load. The other two sensors are used either for sensing the active filter current in case of adopting direct current control strategy in which the switching algorithm controls the active filter currents, or these sensors are used for sensing the supply currents in case of adopting the indirect current control strategy in which the switching algorithm controls the supply currents. The gains of current transformers LOS200D15 used in this circuit can be changed with a variable resistor and TL082 operational amplifier.



Fig.5 the IGBT modules



Fig.6 active filter inductor



Fig.7 D.C. bus capacitor

It is worth mentioning that these currents are fed to the Analog to Digital Converters (ADCs) in TMS320F2812. As the ADCs only accept positive voltage, D.C. offset must be added in case of measuring A.C. quantities. The D.C. offset is taken as $1.65V$ as the maximum operating voltage of the ADCs is $3.3V$. Figure 8 shows the components of the currents measuring circuit. Regarding the voltage measuring circuit, some control strategies require measuring the PCC voltages such as SDM and IRPT.

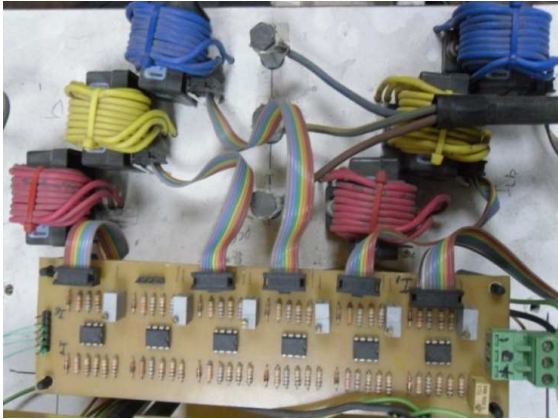


Fig.8 current measuring circuit

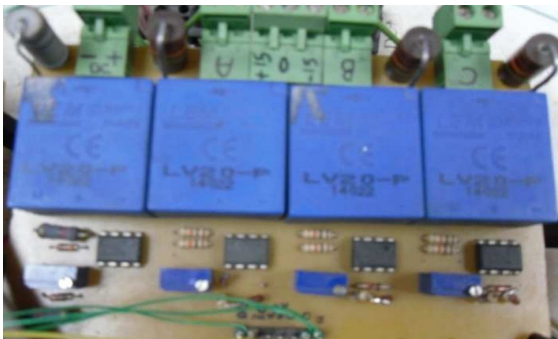


Fig.9 voltage measuring circuit



Fig.10 conditioning circuit



Fig.11 isolation circuit

On the other hand, some control strategies need not to measure the PCC voltages such as SRF. D.C. bus voltage measurement is required in all control strategies. This board has 4 voltage transducers so as to be used with any control strategies. The gains of the voltages transducers (LV20-P) can be changed in the same manner mentioned in the previous section. The presence of the D.C. offset is a must also in this board. This board also contains a zero crossing detectors which can be used to generate a reference sine waves used in forming the reference supply currents. Also, zero crossing detectors are used to synchronize the operation of the software with the supply voltages in some approaches. Figure 9 shows the components of the voltages measurements board.

Regarding, the conditioning circuit, it consists of four parts. The first one is the main power supply. The second one is the level shifter which shifts the logic level from TTL level (output of the DSP) to CMOS level to increase the noise immunity. The third one is the dead time control to prevent the simultaneous operation of any two IGBT switches in the same leg. The design of the dead time is based upon the worst conditions in the turn-off time. A simple R-C circuit with and gates are used to make the desired dead time. The last part is a ULN2003 IC which performs the role of driver current buffer. Figure 10 shows the conditioning circuit board.

Regarding the opto-couplers and isolated power supply circuit, the switching signals generated from the driver IC (ULN2003) is transmitted to the power IGBT through fast six Opto-couplers (HCPL-4504). In the same time, the fault signals from the intelligent power modules are transmitted through six slow Opto-couplers (PC817) to provide the protection against short circuits. Figure 11 shows the components of this board.

Regarding the DSP, The APF is controlled by a Texas Instruments (TI) TMS320F2812 32 bits fixed point chip, it is a member of the TMS320C2000 DSP platform with fixed point. It operates at 150MHz. It is source code compatible to the 24x/240x DSP devices and, additionally, the C28x is a very efficient C/C++ engine, enabling users to develop not only their system control software in a high-level language, but also enables math algorithms to be developed using C/C++. In this paper, Matlab/Simulink libraries are used to develop the software required to run the shunt APF. Figure 12 shows the DSP kit used in this paper. Figure 13 shows the overall control system.

Figure 14 shows the block diagram of the software blocks used in Matlab/Simulink. The first part after

measuring the voltages and/or currents is the detection algorithm. The second part is the D.C. bus voltage controller. In this software, a digital proportional-Integral (P-I) controller is used and is tuned based on the linear model described in [25]. This paper is concerned with the harmonic extraction part in the APF blocks, so the simplest possible model is used without inserting any type of non-linearities or uncertainties. The third part is the switching technique. The switching technique used in this software is the hysteresis band controller. Figure 15 shows the working principle of the hysteresis band controller. The hysteresis band (H) is selected based upon the desired maximum switching frequency.

6 Experimental Results

In this part, the APF performance is investigated under the three different detection algorithms. The code is written using Matlab. Then, it is converted using code composer studios v3.1 to C language. The computer is connected to the DSP using parallel port to download the software. The experimental results are collected using TeKtronix THS720P oscilloscope.

6.1 Synchronous Detection Method

First, SDM software is downloaded and tested. Figure 16 shows the phase (a) load current which contains the harmonic spectrum shown in Fig.17. The harmonic spectrum is obtained using a programmed M-file and power GUI block. Figure 18 shows the phase (a) supply current after compensation. The supply current is distorted which is clear from Fig.19 that shows the harmonic spectrum of the supply current. The 5th, 7th, 11th harmonics contents are compared in table 1. This technique is successful in reducing the lower order harmonics frequencies such as 5th, 7th. However, the impact of the low switching frequency on the compensation process using this technique appears on higher order harmonics such as 11th, 13th,... that amplifies it from 0.4 to 0.43A and from 0.1 to 0.19A respectively. The supply P.F. is increased from 0.852 to 0.895. Figure 21 shows the D.C. bus voltage which is controlled to be 140V which is the same for all the detection techniques. Figure 22 shows the switching pattern of switch number 1. It is obvious that the switching frequency is low at the peaks and high at the sides of the sine wave. It is clear that there is a limiting value on the switching frequency. This value depends on the length of the algorithm in addition to the number of analog to digital conversions used. In this technique, the A.C. voltages are measured.



Fig.12 DSP kit

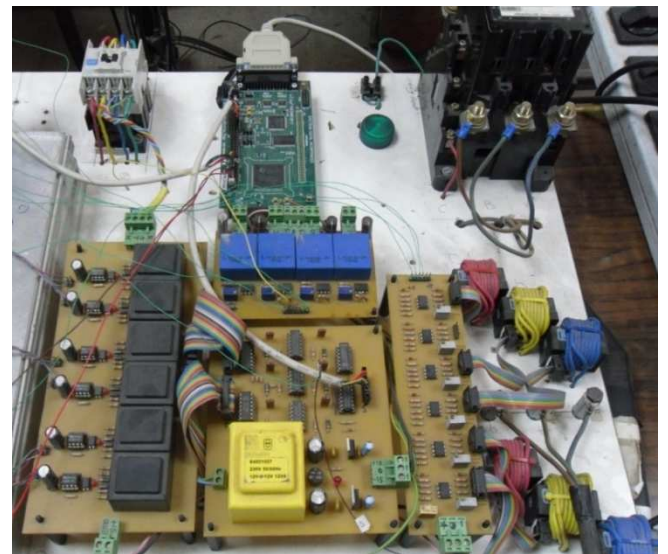


Fig.13 the overall control system

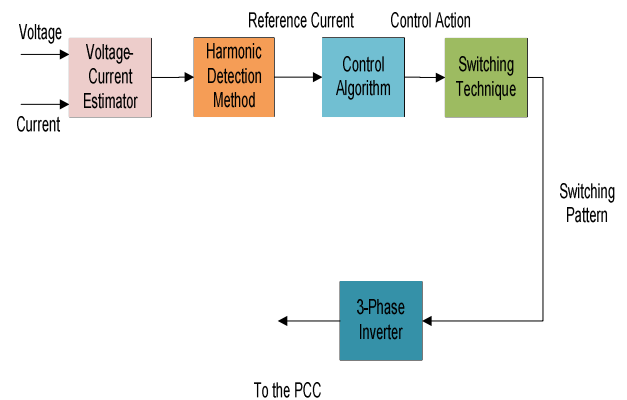


Fig.14 block diagrams of the system

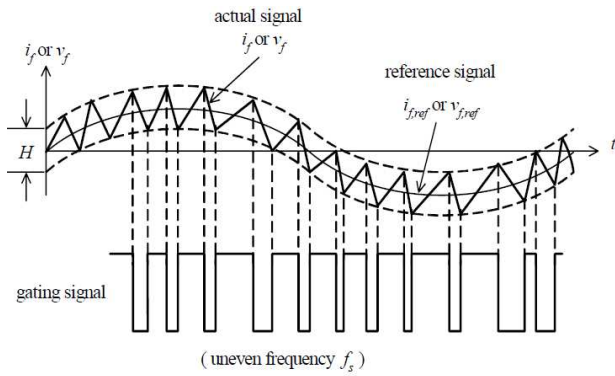


Fig.15 hysteresis controller

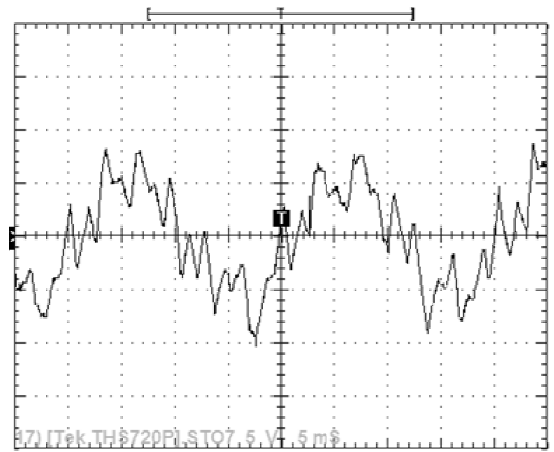


Fig.18 phase (a) supply current

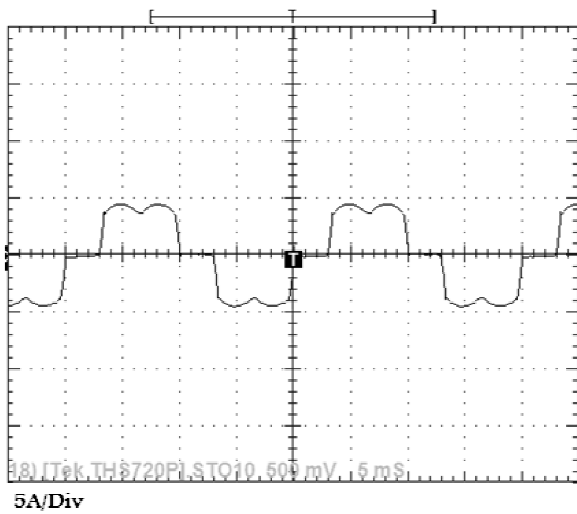


Fig.16 phase (a) load current

Table 1 Comparison between the supply current before and after compensation with SDM

	5 th	7 th	11 th	Fundamental	THD %
Before compensati	1.1	0.4	0.4	4.672	26.95 %
After compensati	0.96	0.15	0.43	5.68	25.68 %

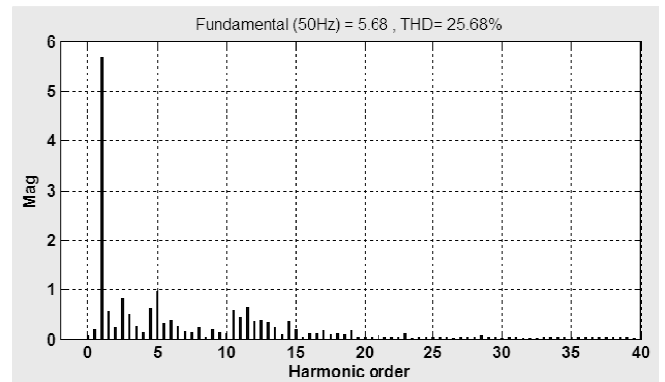


Fig.19 THD of the supply current in SDM

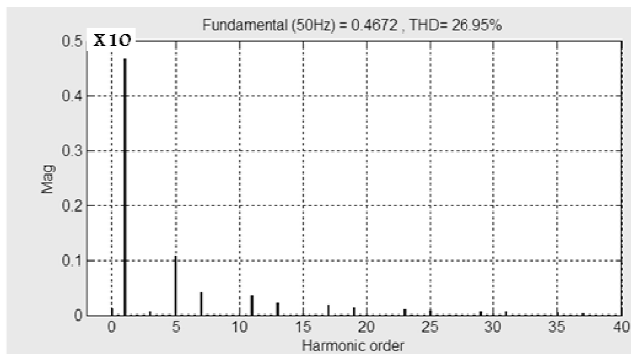


Fig.17 THD of the load current

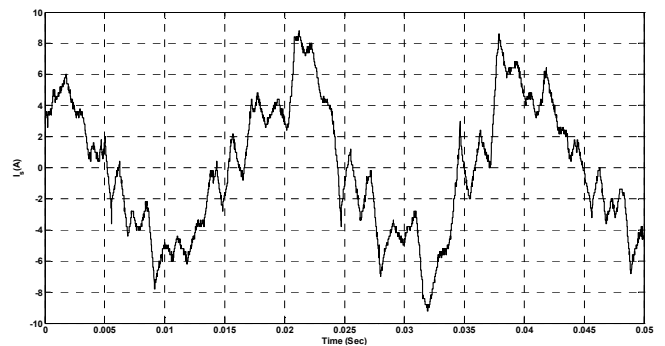


Fig.20 phase (a) supply current from Simulink when running at 175µsec sampling

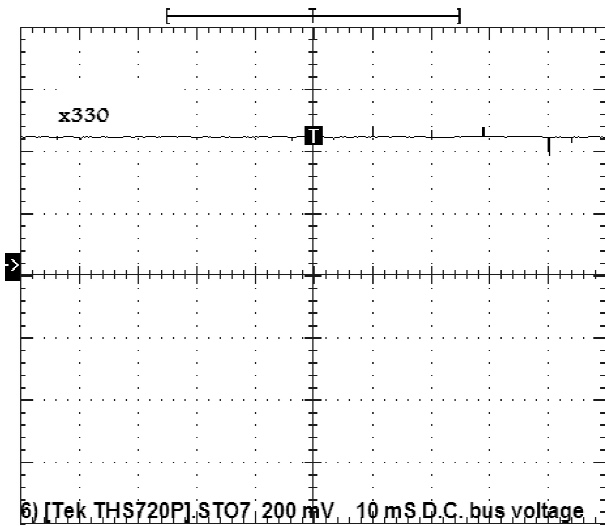


Fig.21 D.C. bus voltage for all algorithms

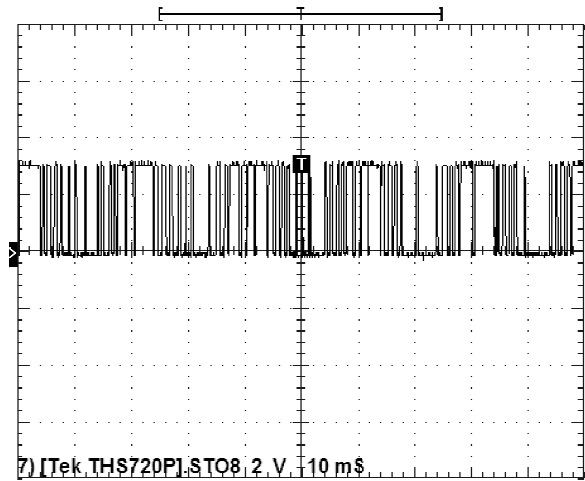


Fig.24 switching pattern of switch1 in IRPT

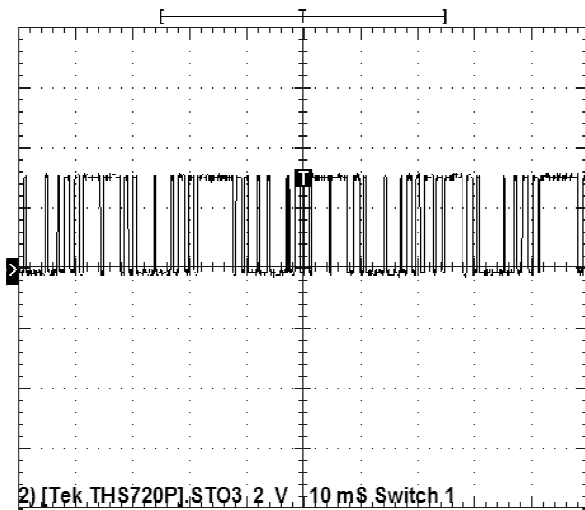


Fig.22 switching pattern of switch1 in SDM

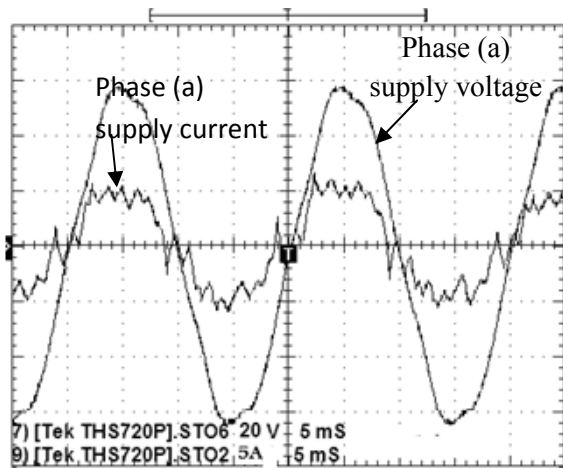


Fig. 23 phase (a) supply current and voltage using IRPT

6.2 Instantaneous Reactive Power Theory

Second, IRPT software is downloaded and tested. Although the IRPT needs to sense the supply voltages, it requires less sampling time. The explanation of that is as follows; the blocks needed in the SDM such as peak calculation needs more time to be implemented on DSP. The minimum sampling time needed for the IRPT is around $146\mu s$. so, the switching frequency is expected to be higher than that of the SDM, and that in turn will reflect on the phase (a) current THD. Figure 23 shows phase (a) current and voltage in case of applying IRPT algorithm. Reducing the sampling time from $175\mu s$ to $146\mu s$ (16.5% reduction) allows the controller to take more samples. So, it increases the accuracy of the calculation. In addition, it increases the maximum switching frequency from 5.8KHz to 6.8KHz. Figure 24 shows the switching pulses to switch 1.

The increased switching frequency leads to better performance in the supply current shape and THD%. Figure 25 shows the harmonic spectrum of the supply current and THD%. The 5th, 7th, 11th harmonics contents are compared in table 2. Due to the inaccurate switching the Fundamental component is above its desired value but it is better than that of SDM. The supply P.F. is increased from 0.852 to 0.91. Figure 26 show the simulation result when running at the same switching frequency.

6.3 Synchronous Reference Frame

Finally, the SRF algorithm is downloaded and tested. As there is no need to measure the supply voltages in this algorithm, the Analog channels needed to implement this algorithm is reduced from 7 channels

in SDM and IRPT algorithm to only 5 channels in SRF algorithm.

The reduction in the number of analog conversions needed clearly reflects in the size of the software and the ability of DSP to perform faster. As a result the minimum sampling time is reduced from 175 μ s and 146 μ s in SDM and IRPT respectively to 125 μ s (28.5% reduction from the SDM) in case of SRF. This reduction gives as mentioned earlier a space to the DSP to take more samples in order to confine the calculation in addition to the enhanced ability of DSP to take faster actions and that in turn increases the switching frequency and reduces the THD%.

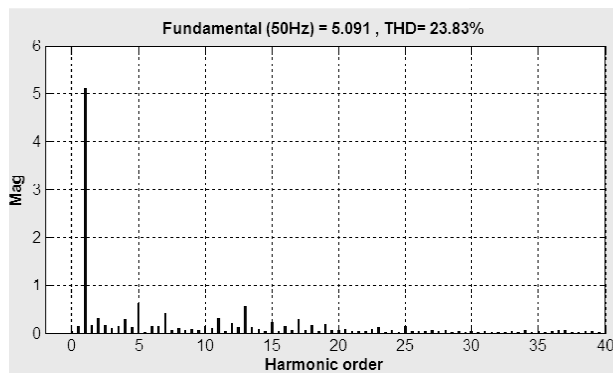


Fig.25 phase (a) supply current harmonic spectrum for the IRPT

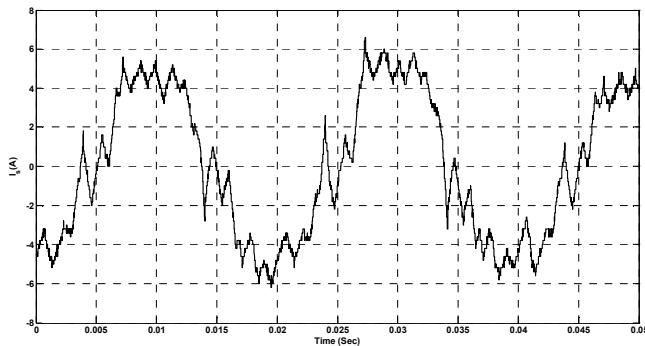


Fig.26 phase (a) supply current from Simulink when running at 146 μ sec sampling

Table 2 Comparison between the supply current before and after compensation with IRPT

	5 th	7 th	11 th _h	Fundamental	THD %
Before compensati	1.1	0.4	0.4	4.672	26.95 %
After compensati	0.6	0.4	0.2	5.091	23.83 %

Figure 27 shows phase (a) supply current and voltage. It is clear that the phase (a) supply current is more related to the sinusoidal shape and in phase with the supply voltage.

Figure 28 shows the switching pulses to switch 1. The maximum switching frequency increases to 8 KHz.

Figure 29 shows that the supply current in SRF is, somehow, recovers the problems associated with those currents produced by SDM and IRPT. Due to the increased switching frequency, the current gets better in the parts which the current reaches the zero values. The sudden changes that appear in the supply current are due to the lower supply inductance. The supply P.F. is increased from 0.852 to 0.942. Figure 30 shows the simulation for the supply current. It is clear that this technique gives also the nearest value to the desired supply current as it results in fundamental component of 4.262A and the desired value is 4.67A.

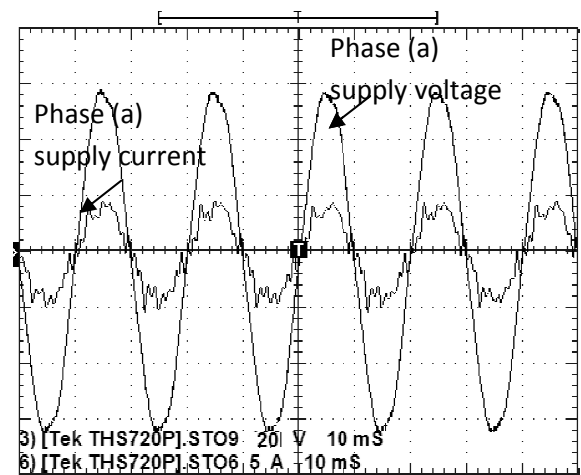


Fig. 27 phase (a) supply current and voltage in SRF

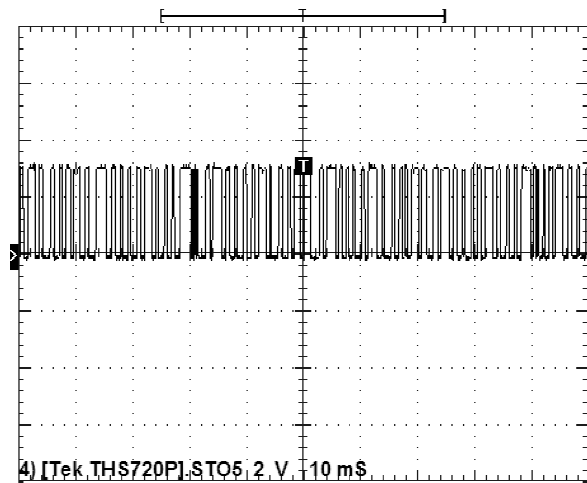


Fig.28 switching pattern of switch1 in SRF

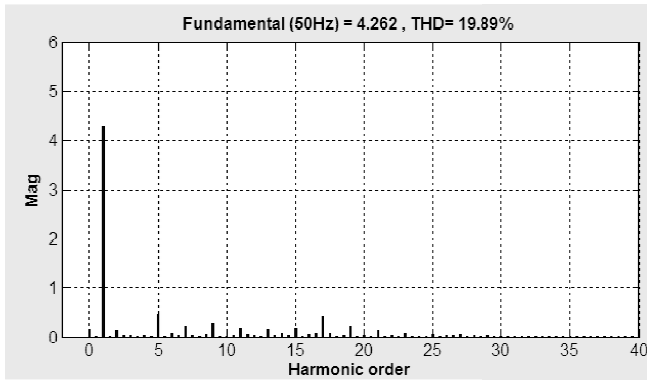


Fig.29 phase (a) supply current harmonic spectrum for the SRF

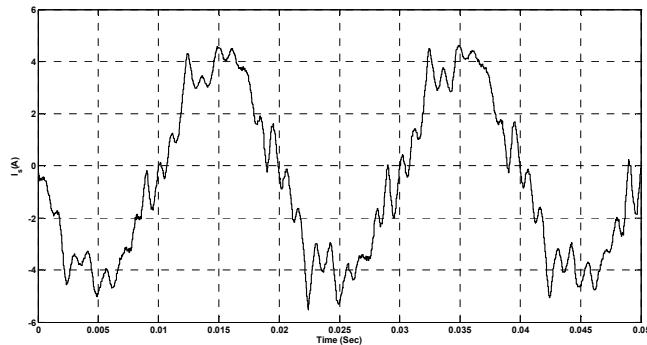


Fig.30 phase (a) supply current from Simulink when running at 125µsec sampling

Table 3 Comparison between the supply current before and after compensation with SRF

	5 th	7 th	11 ^t _h	Fundamental	THD %
Before compensati	1.1	0.4	0.4	4.672	26.95 %
After compensati	0.4	0.1	0.2	4.262	19.89 %

Table 3 compares between the supply current before and after compensation in IRPT. From the experimental results we can see that the DSP gives some limitations on the maximum switching frequency which limits the performance of the APF from THD and P.F. points of view. These limitations come from the minimum allowable sampling time. The minimum allowable sampling time is a strong function in the code size and the number of used sensors. Programming the DSP with Simulink increases the code size which limits the switching frequency. SRF has the best performance because it uses the smallest number of sensors. The effect of sampling time on the performance of the APF is

proved when running the simulation at the sampling times used in the experimental setup.

7 Conclusion

Shunt APF is constructed and tested successfully in this paper. Three different detection algorithms are used. This algorithms result finally in graded performance for the shunt APF. The graded performance is due to the complexity and the length of the algorithm. SRF has the lowest THD% and the highest P.F. due to the small number of sensors used in this algorithm. IRPT results in a moderate performance. SDM has the worst performance. The graded performance does not mean that; SDM and IRPT are not successful algorithms, but they need more powerful DSP or to develop the codes needed in C directly rather than compiling from Simulink to C language. That will reduce the code size which will lead to smaller sampling time and better switching frequency resulting finally in better THD and P.F.

References:

- [1] "IEEE Recommended Practices and Requirements for Harmonic Control in Electrical Power Systems," *IEEE 519-1992*.
- [2] L. Gyugyi, and E. C. Strycula, "Active AC Power Filters", in *Proceeding of IEEE/IAS Annual Meeting*, pp. 81-87, 1976.
- [3] Y. Han, Mansoor, G. Yao, L. Zhou, C. Chen "Harmonic Mitigation of Residential Distribution System using a Novel Hybrid Active Power Filter" *WSEAS Transactions on Power Systems*, Issue 12, Volume 2, December 2007, pp 250-260.
- [4] M. El-Habrouk, M. Darwish, and P. Mehta, "Active Power Filters: A Review", in *proceeding of IEEE Electric Power Applications*, Vol. 147pp. 403-413, Sep. 2000,.
- [5] B. Singh, K. Al-Haddad, A. Chandra, "Active Power Filter for Harmonic and Reactive Power Compensation in Three-Phase, Four-Wire Systems Supplying Non-Linear Loads" *ETEP - Eur. Trans. Elect. Power Eng*, Vol. 8, no. 2, , pp. 139-145, Mar/April 1998.
- [6] L. Asiminoaei, F. Blaabjerg, and S. Hansen "Detection is key - Harmonic Detection Methods for Active Power Filter Applications" *IEEE industry applications magazine* july|aug 2007.
- [7] D. Chen, and S. Xie " Review of the control strategies applied to active power filters" in *proceeding of IEEE International Conference on Electric Utility Deregulation, Restructuring and*

- Power Technologies (DRPT2004)* Hong Kong, April 2004
- [8] K-L. Areerak, "Harmonic Detection Algorithm based on DQ Axis with Fourier Analysis for Hybrid Power Filters", *WSEAS Transactions on Power Systems*, Issue 11, Volume 3, November 2008, pp. 665-674.
- [9] S. Prasad, K. Prasad, and N. Enjeti "control strategies for active power filter in three-phase four-wire" in *proceeding of Power Electronics Specialist Conference, PESC '03. IEEE 34th Annual 2003 Acapulco, Mexico, 2003*.
- [10] G. Chang, Senior, and T. Shee " A Novel Reference Compensation Current Strategy for Shunt Active Power Filter Control" *IEEE transactions on power delivery*, Vol. 19, no. 4, October 2004.
- [11] H. Li, F. Zhuo, Z. Wang, . Lei, and L. Wu " A Novel Time-Domain Current-Detection Algorithm for Shunt Active Power Filters" *IEEE transactions on power systems*, Vol. 20, no. 2, may 2005.
- [12] W. Grady, M. Samotyj, and A. Noyola, "Survey of active power line conditioning methodologies", *IEEE Trans. on Power Delivery*, Vol. 5, Issue 3, pp. 1536 – 1542, 1990.
- [13] O. Solomon, "The use of DFT windows in signal-to-noise ratio and harmonic distortion computations", *IEEE Trans. on Instrum. And Measur.*, Vol. 43, Issue 2, pp. 194 – 199, 1994.
- [14] M. El-Habrouk, and M. Darwish, "Design and implementation of a modified Fourier analysis harmonic current computation technique for power active filters using DSPs in *proceeding of Electric Power Applications*, Vol. 148, pp. 21 – 28, 2001.
- [15] S. Srianthumrong, and S. Sangwongwanich, "An active power filter with harmonic detection method based on recursive DFT", in *proceeding of Harmonics and Quality of Power*, Vol. 1, 1998, pp. 127 – 132, 1998.
- [16] A. Girgis, W. Chang, and E. Makram, "A digital recursive measurement scheme for online tracking of power system harmonics", *IEEE Trans. on Power Delivery*, Vol. 6, Issue 3, pp. 1153 – 1160, 1991.
- [17] H. Akagi, Y. Kanazawa, and A. Nabae, "Generalized Theory of the Instantaneous Reactive Power in Three-Phase Circuits", in *proceeding of IPEC'83 - Int. Power Electronics Conf.*, Tokyo, Japan, pp. 1375-1386, 1983.
- [18] H. Akagi, E. Watanabe, and M. Aredes, "Instantaneous Power Theory and Applications to Power Conditioning", Wiley-IEEE Press 2007, Chap.3.
- [19] M. Aredes, and E. Watanabe, "New Control Algorithms for Series and Shunt Three-Phase Four- Wire Active Power Filters", *IEEE Trans. Power Delivery*, Vol. 10, no. 3, pp. 1649-1656, July 1995.
- [20] M. Amer, S. Zaid, and O. Mahgoub "Power Quality Improvement Using APF for Industrial Loads" *Master Thesis*, Cairo University, Chap.4, January 2010.
- [21] S. Bhattacharya, D. Divan and B. Banerjee, "Synchronous Frame Harmonic Isolator Using Active Series Filter", *EPE'91 Conference Records*, pp. 30-35, 1991.
- [22] C. Lin, C. Chen, C. Huang, "Reactive and Harmonic Current Compensation for Unbalanced Three-phase Systems", *IASTED Power High Tech Conference*, Tainan, Taiwan pp. 317-321, March 1991.
- [23] M. Shousha, S. Zaid, and O. Mahgoub, " Better Performance for Shunt Active Power Filters" in *proceeding of International Conference on Clean Electrical Power ICCEP2011, Italy, pp.56-62, 2011*.
- [24] M. Shousha, S. Zaid, and O. Mahgoub, "A Time Domain Harmonic Reference Estimation for Shunt Active Power Filters under Non-Ideal Mains Voltages" in *proceeding of International Conference on Electrical and Computer Engineering, ICECE2011, Malaysia, pp.456-462, 2011*.
- [25] V. Belov, N. Paldyaev, A. Shamaeva, A. Johansson, P. Leisner, I. Belov "Matlab / Simulink Model of an Active Power Filter Based on Multi-stage Inverter Architecture" *Proceedings of the 5th WSEAS Int. Conf. on Power Systems and Electromagnetic Compatibility, Corfu, Greece, August 23-25, 2005*, pp44-48.